Polymer 50 (2009) 3119–3127

Contents lists available at ScienceDirect

Polymer

journal homepage: www.elsevier.com/locate/polymer

Synthesis and characterization of itaconic anhydride and stearyl methacrylate copolymers

Shurui Shang [a], Samuel J. Huang [b,c], R.A. Weiss [a,b,*]

[a] Department of Chemical Materials and Biomolecular Engineering, University of Connecticut, Storrs, CT 06269-3136, USA
[b] Polymer Science Program, University of Connecticut, Storrs, CT 06269-3136, USA
[c] Department of Chemistry, University of Connecticut, Storrs, CT 06269-3136, USA

ARTICLE INFO

Article history:
Received 10 March 2009
Received in revised form
4 May 2009
Accepted 6 May 2009
Available online 18 May 2009

Keywords:
Sustainable
Synthesis
Comb polymers

ABSTRACT

The free-radical copolymerization and the properties of comb-like copolymers derived from renewable resources, itaconic anhydride (ITA) and stearyl methacrylate (SM), are described. The ITA–SM copolymers were nearly random with a slight alternating tendency. The copolymers exhibited a nanophase-separated morphology, with the stearate side-chains forming a bilayer, semi-crystalline structure. The melting point (T_m) of the side-chains and the crystallinity decreased with increasing ITA concentration. The crystalline side-chains suppressed molecular motion of the main chain, so that a glass transition temperature (T_g) was not resolved unless the ITA concentration was sufficiently high so that $T_g > T_m$. The softening point and modulus of the copolymers increased with the increasing ITA concentration, but the thermal stability decreased.

1. Introduction

Polymers based on renewable resources such as plant and agro-industrial waste are of considerable interest as substitutes for petroleum-based materials. Such materials are attractive from an environmental perspective, especially if they are biodegradable. Lactic acid is a monomer obtained from the fermentation of carbohydrates, and poly(lactic acid) (PLA) is a biodegradable plastic that has recently gained acceptance as a commodity thermoplastic [1,2].

Itaconic anhydride (ITA) and stearyl methacrylate (SM) are other monomers obtained from renewable resources. ITA is produced from the pyrolysis of citric acid or through the fermentation of carbohydrates forming itaconic acid followed by its dehydration to form the anhydride [3], and SM is derived from renewable plant oils [4–6]. ITA can be polymerized [6–8] or copolymerized with various other monomers [9–15] by free-radical reactions. Because it forms highly reactive tertiary radicals [11–13], ITA is more reactive than maleic anhydride and is an alternative monomer for introducing polar functionality into polymers. Poly(SM) and copolymers of SM and other acrylate monomers have also been reported [16–19].

The free-radical copolymerization of ITA and SM was previously described by Wallach [14] but the properties of those materials were not characterized and the work was not published. The present paper is part of a research program directed at preparing ionomers from renewable monomers. That research is motivated by an interest in introducing polar functionality onto relatively non-polar biopolymers such as PLA to increase the glass transition temperature, T_g, to improve adhesion and compatibility with more polar substrates or polymers, to provide polar grafting sites for biodegradable scaffolds, and for preparing amphiphilic polymers for drug release applications.

2. Experimental details

2.1. Materials

SM, ITA and anhydrous ethyl acetate (EA) were obtained from Aldrich Chemical Co. The SM and EA were determined to be pure by ^{1}H NMR and FTIR and were used as received. ITA was re-crystallized from dry toluene. Azobisisobutyronitrile (AIBN), obtained from Aldrich Chemical Co., was re-crystallized from methanol.

2.2. Synthesis of ITA–SM copolymers

The copolymerization procedure followed the free-radical reaction described by Wallach [14]. The reaction scheme is depicted in Fig. 1. ITA has a higher reactivity than itaconic acid [11], but it is easily hydrolyzed by water. In order to retain the anhydride functionality in

* Corresponding author. Institute of Materials Science, University of Connecticut, 97 N. Eagleville Rd., Storrs, CT 06269-3136, USA.
E-mail address: rweiss@ims.uconn.edu (R.A. Weiss).

0032-3861/$ – see front matter © 2009 Elsevier Ltd. All rights reserved.
doi:10.1016/j.polymer.2009.05.012

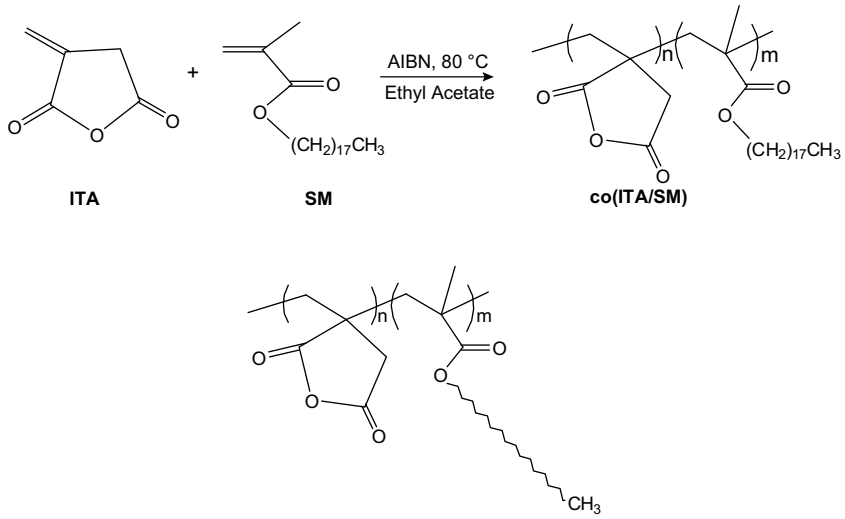

Fig. 1. Copolymerization of itaconic anhydride (ITA) and stearyl methacrylate (SM).

the copolymer, all the glassware and reactants was dried before copolymerization, and anhydrous ethyl acetate was used as the solvent. Various molar ratios of ITA and SM were dissolved in EA at 80 °C in a round-bottom flask equipped with a magnetic stir bar and a condenser with a desiccant outlet and a nitrogen inlet. The total monomer concentration was 66.7 wt%, and the initiator (AIBN) concentration was 4 mol% based on the concentration of the two comonomers. The reactions were carried out at 80 °C for 12 h with stirring under a nitrogen atmosphere. After the polymerizations were completed, the reaction solution was precipitated at −20 °C in either hexane for an ITA feed concentration >70 mol% or methanol for an ITA feed concentration ≤70 mol%. The precipitate was filtered, washed with additional hexane or methanol at ambient temperature and dried in a vacuum oven for 48 h. The copolymers were re-precipitated from a 30% (w/v) solution in EA with excess hexane or methanol at −20 °C, filtered, and dried in a vacuum oven. The copolymers produced are listed in Table 1. The general nomenclature used for the copolymers is *x.yITA–SM*, where *x.y* = the mol% ITA. PSM and PITA are the SM and ITA homopolymers.

Physical mixtures of ITA and SM were also prepared for comparison by dissolving the two monomers in anhydrous THF, stirring the solution and allowing the solvent to completely evaporate. The solvent evaporation was carried out over calcium sulfate in a desiccator at room temperature and under a flow of dry N_2 to prevent hydrolysis of the ITA.

2.3. Polymer characterization

Fourier transform infrared spectroscopy, FTIR, (Nicolet 560 Magna spectrometer) was used to determine the copolymer composition using either solid films or mull samples. The mulls were prepared by mixing the polymer with dry KBr powder and pressing into a transparent KBr pellet. Solid films were prepared by solution casting the polymer onto a KBr pellet followed by evaporation of the solvent.

Table 1
Characteristics of ITA–SM Copolymerizations.

Sample notation	Feed mole ratio ITA/SM	[ITA] in copolymer (mol%)	M_n (kg/mol)	PDI	Yield (%)
PSM	0/100	0	57.1	2.28	95.6
22.1ITA–SM	5/95	22.1	45.1	1.90	79.3
37.8ITA–SM	15/85	37.8	33.0	1.85	68.5
56.0ITA–SM	30/70	56.0	34.8	1.88	82.4
59.2ITA–SM	50/50	59.2	29.1	1.82	88.2
70.1ITA–SM	70/30	70.1	24.1	1.79[a]	74.9
87.4ITA–SM	85/15	87.4	29.6	2.45[a]	59.9
PITA	100/0	100	27.9	1.44	47.5

[a] After extracting oligomers (see text).

A differential scanning calorimeter, DSC, (TA instrument Q100) was used to measure the thermal transitions and crystallinity of the samples. Specimens of 5–10 mg were encapsulated in aluminum pans and heated or cooled between −60 °C and 180 °C under dry nitrogen at a rate of 10 °C/min. The melting point, T_m, was defined as the peak temperature of the melting endotherm and the glass transition temperature, T_g, was taken as the midpoint of the heat capacity change at the transition. Thermogravimetric analysis, TGA, (TA instruments Q500) was carried out under a nitrogen atmosphere from room temperature to 900 °C and a heating rate of 10 °C/min. Thermomechanical analysis, TMA, (Perkin–Elmer TMA7) was performed under a helium atmosphere using a penetration probe. Rectangular film samples of ~1 mm thick were prepared by compression molding under vacuum. A force of 60 mN was applied to the probe, and the samples were heated at a rate of 5 °C/min from −125 °C until the probe penetrated through the sample.

Molecular weight averages were measured by gel permeation chromatography, GPC, (Waters 150-C ALC) using a flow rate of 1.0 mL/min and an evaporative light scattering detector. The analysis was performed at 35 °C using high-performance liquid chromatography-grade THF as the eluent. Polystyrene standards were used to calibrate the molecular weight.

Wide angle X-ray diffraction, WAXD, (Bruker D5005 X-ray diffractometer) measurements were made at room temperature using solid powder samples, Cu K_α ($\lambda = 0.154$ nm) radiation at 40 kV and 40 mA, a Ni filter and an angular range of $2\theta = 10$–$90°$. The scattering vector, q, was calculated from $q = 4\pi\sin\theta/\lambda$, where 2θ = the scattering angle and λ = the wavelength of the X-rays. The periodicity (d-spacing) corresponding to the peak in the X-ray pattern was calculated from Bragg's law, $d = 2\pi/q$. Small angle X-ray scattering, SAXS, data were obtained using a Bruker Small-Angle Scattering Instrument with a Rigaku Ru-300 rotating anode generator (Cu K_α radiation) and a HiStar 2D detector. Two-dimensional (2D) WAXD experiments were performed at the synchrotron X-ray beam line X27C at the National Synchrotron Light Source, Brookhaven National Laboratory, using an X-ray wavelength of 0.1371 nm. Temperature-resolved X-ray data were obtained using an Instec HCS410 hot stage equipped with a liquid-nitrogen cooling accessory as the temperature control system and Fuji imaging

plates. The typical data acquisition time was 60 s and 2D image data files were obtained using a Fuji BAS-2500 scanner. The scattering angle was calibrated using Al_2O_3. One-dimensional (1D) WAXD curves were calculated by averaging the intensity over the azimuthal angle at each scattering angle.

3. Results and discussions

The copolymerization reaction was monitored by FTIR analysis. The IR spectra of the SM and ITA monomers, a physical mixture of the two monomers (ITA/SM = 30/70 mole ratio) and the 59.2ITA–SM copolymer are shown in Fig. 2. The spectrum of the ITA and SM monomer mixture was a simple addition of the individual spectra for ITA and SM. The absorptions for the ITA are at 1780 and 1856 cm^{-1} (C═O symmetric and asymmetric stretching of the 5-member anhydride unit), 1660 cm^{-1} (C═C stretching), and 1400 cm^{-1} (═CH_2 in plane deformation), and for SM at 1720 cm^{-1} (C═O) and 1630 cm^{-1} (C═C). For the copolymer, the absorption bands associated with the C═C double bonds at 1400, 1630 and 1660 cm^{-1} disappeared, confirming the polymerization. The peaks for the anhydride ring vibrations in the copolymer are at 1782 and 1862 cm^{-1} and the carbonyl stretching of the SM moved to 1730 cm^{-1}. The anhydride peaks indicate that the anhydride remained intact in the copolymer, and the shift to higher frequency (higher energy) of the SM carbonyl stretch is consistent with the elimination of the conjugation of the vinyl and carbonyl double bonds.

The molecular weight of the copolymers decreased with increasing ITA concentration in the feed, see Table 1, which may be a consequence of the allylic hydrogen in ITA that can act as a chain transfer agent in radical polymerization [20]. Tomic et al. [21] reported that the kinetic constants for chain transfer to monomer of dialkyl itaconates are nearly two orders of magnitude greater than those of alkyl methacrylate. In fact, the molecular weight and yield for the homopolymerization of ITA in this study were much lower than for the homopolymerization of SM and the ITA-SM copolymers when the feed was rich in SM, see Table 1. For feed compositions of less than 70% ITA, GPC indicated that only copolymer was produced. For feed compositions greater than 70% ITA, however, the GPC curve showed both the presence of copolymer at low elution times and ITA oligomers at high elution times, see Fig. 3. The latter was confirmed by FTIR and X-ray analyses of the material extracted with acetone. This paper focuses only on the polymer products. Where necessary, residual ITA monomer was extracted before analysis of the copolymer. The PSM sample exhibited a bimodal molecular weight distribution. The reason for that is not known, but since PSM was not the focus of this research, an investigation of the polymerization of SM was not carried out.

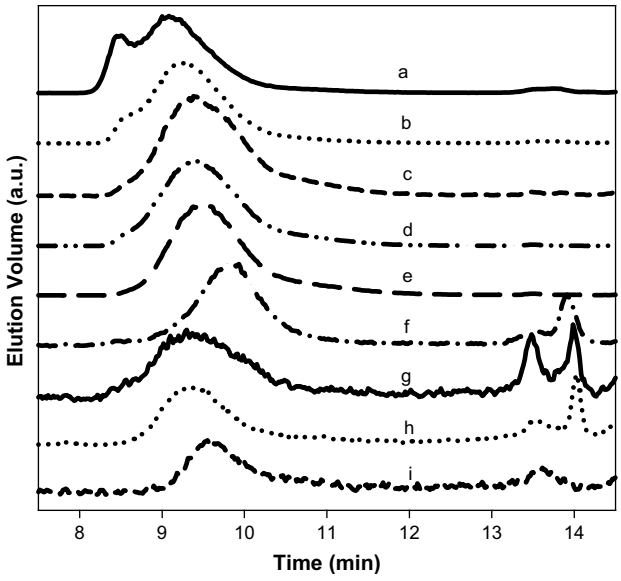

Fig. 3. GPC curves for products of ITA–SM copolymers as a function of feed composition (mol/mol): (a), 0/100 ITA/SM; (b), 5/95; (c), 15/85; (d), 30/70; (e), 50/50; (f), 70/30; (g), 85/15; (h), 95/5; (i), 100/0. Curves are displaced vertically for clarity.

The copolymer compositions were determined from a calibration curve prepared from the FTIR spectra of physical mixtures of different compositions of ITA and SM, using the ratio of the bands at 1856 cm^{-1} for ITA (C═O stretching of the carbonyl in the anhydride ring) and 1720 cm^{-1} for SM (C═O stretching), see Fig. 4. The corresponding bands for the copolymers were shifted slightly in

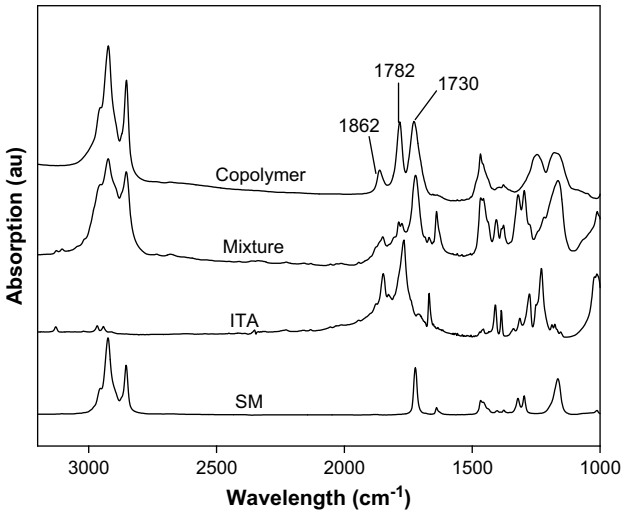

Fig. 2. IR curves of the monomers, a physical mixture of ITA/SM (30/70 mole ratio) and the 59.2ITA–SM copolymer. The data are displaced vertically for clarity.

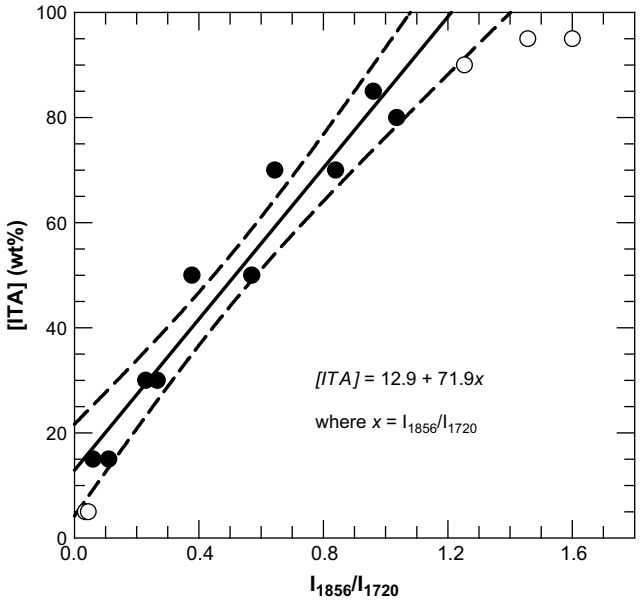

Fig. 4. IR calibration curve of ITA/SM physical mixtures. Each data point represents a single mixture. The solid line is the least squares fit of a second order polynomial and the dashed lines are the 95% confidence intervals.

frequency to the frequencies of 1862 and 1730 cm^{-1} for the monomers, which may introduce small errors in the calculation of the copolymer compositions. Each datum point shown in Fig. 4 represents a separately mixed blend. The solid line in Fig. 4 is a linear least squares fit of the data, which corresponds to Beer's law. The dashed curves are the 95% confidence limits. The data in Fig. 4 exhibit nonlinearity for the samples with compositions with less than 10 wt % of one of the components. That may be a consequence of errors in the measurement of the IR intensities due to inhomogeneities in the physically mixed blends, which were immiscible and the breadth of the IR absorbances. Only the IR data for compositions with at least 15 wt% of one of the components were used to construct the linear fit. That composition range encompassed all of the samples, except 87.4ITA–SM. The 95% confidence limits reflect the uncertainty of the compositions reported in this paper. The calculated copolymer compositions are listed in Table 1. Wallach [14] reported that the reactivity ratios for the copolymerization of ITA and SM were $r_{ITA} = 0.53$ and $r_{SM} = 0.12$, which indicates the formation of a statistical copolymer with slight alternating tendency [22].

At temperatures above 100 °C, ITA can isomerize to citraconic anhydride that inhibits polymerization of ITA [7,23]. To check whether isomerization may have occurred under the reaction conditions used in this study, the unreacted ITA after homopolymerization was recovered from the solution. ^{1}H NMR analysis indicated that no citraconic anhydride (6.78 ppm, 1H for CH; 2.15 ppm, 3H for CH_3 [24]) was formed.

4. Thermal behavior of ITA–SM copolymers

The DSC thermograms for the 2nd heating scan of the homopolymers and copolymer are shown in Fig. 5. For PSM and copolymers with ITA concentrations less than 30 mol%, a single relatively sharp melting peak at 30–33 °C was observed, which indicates that the crystallinity of the copolymer arises from crystallization of the SM side chains. Above 30 mol% ITA, the melting point of the SM side chains in the copolymers and the crystallinity decreased with increasing ITA content, see Table 2. The melting point data are plotted in Fig. 6, and the solid line in Fig. 6 corresponds to the

Table 2
Thermal (DSC) and Thermomechanical analysis (TMA) results for ITA–SM copolymers

Copolymer	[ITA] (mol fraction)	[ITA] (mass fraction)	ΔH_f (J/g SM)	ΔH_f (kJ/mol SM)	% xyl[a]	T_g (°C)	T_m (°C)	n_c	$T_{50\%,TMA}$ (°C)
PSM	0	0	62.8	21.3	1.0	–	30.2	6.9	41.0
22.1ITA–SM	5	0.09	65.4	22.2	1.0	–	30.4	7.2	43.2
37.8ITA–SM	15	0.17	58.3	19.8	0.9	44.4	31.8	6.4	44.4
56.0ITA–SM	30	0.30	42.8	14.5	0.7	53.2	11.9	4.7	67.7
59.2ITA–SM	50	0.32	37.4	12.7	0.6	55.2	5.7	4.1	67.7
70.1ITA–SM	70	0.44	20.0	6.8	0.3	106.5	−10.0	2.2	109.6
87.4ITA–SM	85	0.70	10.6	3.6	0.2	110.1	−22.3	1.1	96.9
PITA	100	1	–	–	–		–	–	–

[a] % Crystallinity relative to PSM.

melting point depression given by equation (1) for a random copolymer with only one crystallizable repeat unit [25,26]:

$$\frac{1}{T_m} - \frac{1}{T_m^o} = -\frac{R}{\Delta H_\mu} \ln x_A \tag{1}$$

where T_m and T_m^o are the melting points of the random copolymer and 100% crystalline homopolymer, respectively; R is the gas constant; ΔH_μ refers to the heat of fusion per mole of repeat units of the 100% crystalline homopolymer; and x_A represents the mole fraction of the crystalline component in the copolymer. Equation (1) requires the equilibrium melting points, which were not measured in this study, but the value of $T_m = 31$ °C for the PSM is not too different from the literature value for icosane ($T_m = 37$ °C) [27], an aliphatic alkane with 18 CH_2 units, so T_m^o was taken as 37 °C for equation (1). That value was chosen instead of the experimental melting point of PSM (31 °C), because the low molecular weight compound probably better reflects the equilibrium melting point of the alkane side-chain in the absence of hindrance from the polymer backbone. Note also that when the experimental T_m for PSM (31 °C) was used for T_m^o, the curve in Fig. 6 was indistinguishable from that using 37 °C, which is a consequence of equation (1) being relatively insensitive to small changes in the absolute temperature used for T_m^o. The heat of fusion was taken as $\Delta H_{SM} = 55.3$ kJ/mol SM, which was calculated by assuming 100% crystallization of the 18 CH_2 with

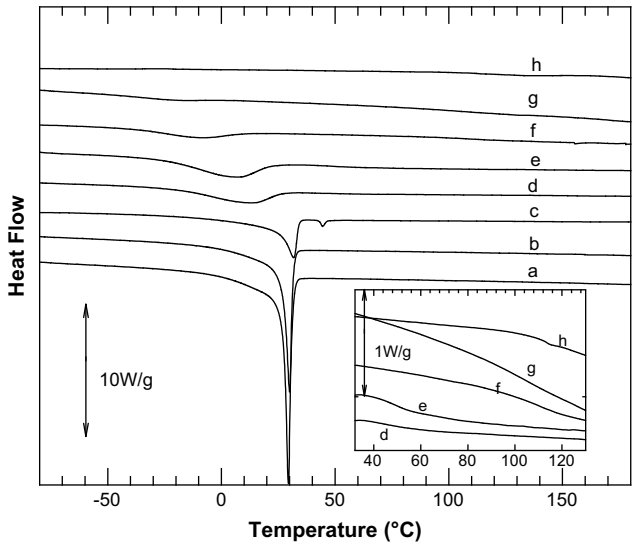

Fig. 5. DSC thermograms of the 2nd heating scan of ITA–SM copolymers: (a) PSM; (b) to (g) ITA concentrations in copolymer are 22.1, 37.8, 56, 59.2, 70.1, and 87.4 mol%, respectively; (h) PITA. Data are displaced vertically for clarity. The inset expands the glass transition region for the materials (see Discussion in text).

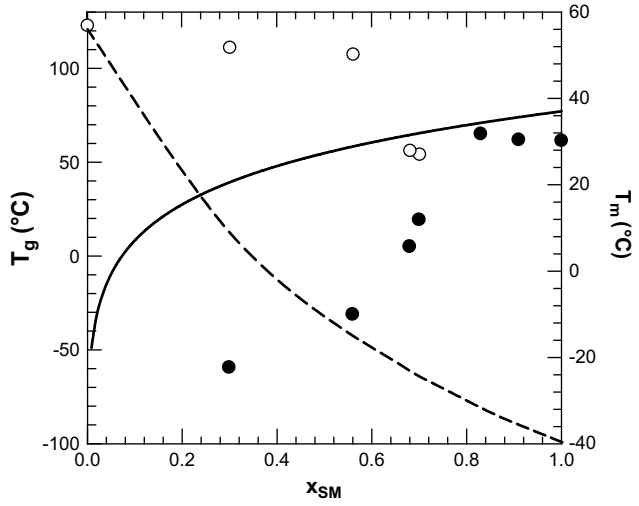

Fig. 6. Thermal transitions vs. composition for ITA–SM copolymers: (○) T_g; (●) T_m. The dashed line is the Fox equation prediction for the T_g of an amorphous random copolymer of ITA and SM, and the solid line represents Flory's melting point prediction for a random copolymer with only one crystallizable unit.

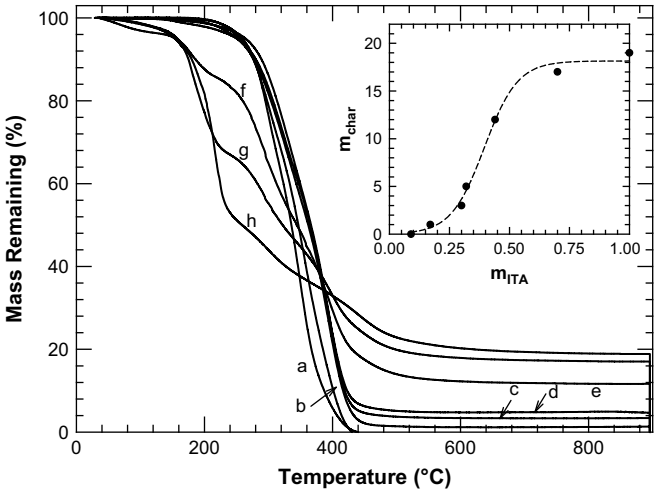

Fig. 7. TGA curves of ITA–SM copolymers. (a) PSM; (b) to (g) ITA concentrations in copolymer are 22.1, 37.8, 56, 59.2, 70.1, and 87.4 mol% respectively; (h) PITA. The inset shows the relationship between the mass fraction of ITA in the polymer and the mass fraction of char at 900 °C. The solid line in the inset is a linear least squares fit of the data and the dotted curves are the 95% confidence limits.

an average melting enthalpy per CH_2 unit for *n*-alkanes $\Delta H_{CH2} = 3.07$ kJ/mol [28].

The experimental T_m values (solid dots in Fig. 6) clearly do not follow the melting point prediction of equation (1), which is further confirmation that the crystallization in these copolymers is due to that of the SM side-chains. The theory for equation (1) was derived for crystallization of a linear chain and not for a side-chain. In the latter case, one might expect the crystallization to depend only on the flexibility of the backbone and the separation of the side chains, and not on the chemistry of the backbone.

The lower melting points and crystallinity of the copolymers with increasing ITA concentration is probably due to the increased difficulty of the side chains to pack efficiently for crystallization when the separation along the chain increases, i.e., the dilution of the side chains, requires larger distances for the side chains to diffuse through a highly viscous melt to crystallize and cooperative motion of the backbone in that the side chains must attain an adequate conformation for crystallization.

Equation (2) provides an estimate of the number of side-chain CH_2 groups (n_c) that crystallize,

$$n_c = \frac{\Delta H_f}{\Delta H_{CH_2}} \tag{2}$$

where ΔH_f is the enthalpy of fusion of the SM in the copolymer and ΔH_{CH_2} is the average melting enthalpy per CH_2 unit for *n*-alkanes [28]. Thus, an average of 6.9 methylene units per side chain participate in the side chain crystallites of PSM, which is higher than the $n_c = 4.7$ reported for PSM by Hempel et al. [29]. For the ITA–SM copolymers, n_c did not change up to a ITA content of ~15 mol%, but then decreased with increasing ITA concentration above ~30 mol% ITA, see Table 2, which supports that conclusion that dilution of the side chains inhibits the ability of the chains to achieve registration for crystallization.

The T_g of the copolymers was poorly resolved. For homopolymer of SM and copolymers with ITA concentration lower than 40 mol%, the DSC analysis found no evidence of a glass transition in the temperature range studied, see Fig. 5(a–c). The T_g of PSM is reported to be about −100 °C [30,31], but it is suppressed by the side chain crystallinity, which makes it difficult to observe experimentally

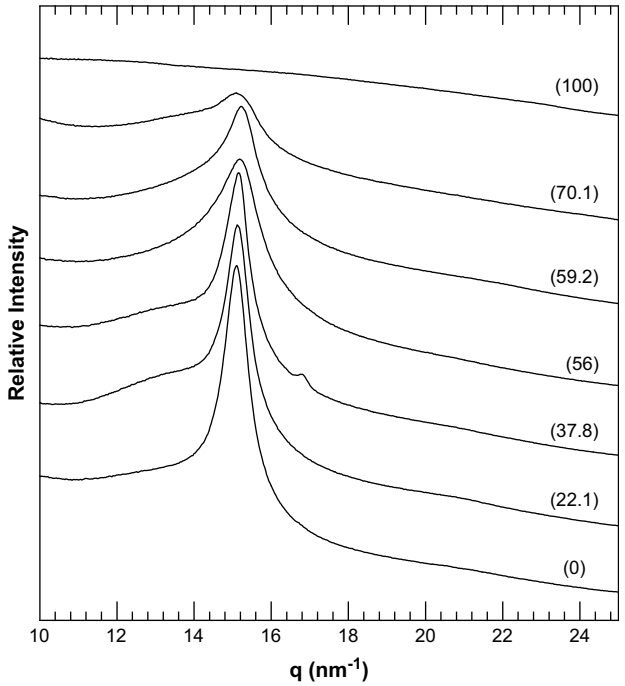

Fig. 8. WAXD curves (BNL synchrotron) for PSM, PITA and ITA–SM copolymers. The numbers in parentheses represent the mol% ITA in the polymer (zero corresponds to PSM, and 100 to PITA). PSM, ITA–SM22.1, ITA–SM37.8, and PITA were measured at 20 °C; the rest of the copolymers were measured at −50 °C, to insure all were measured below their respective T_ms.

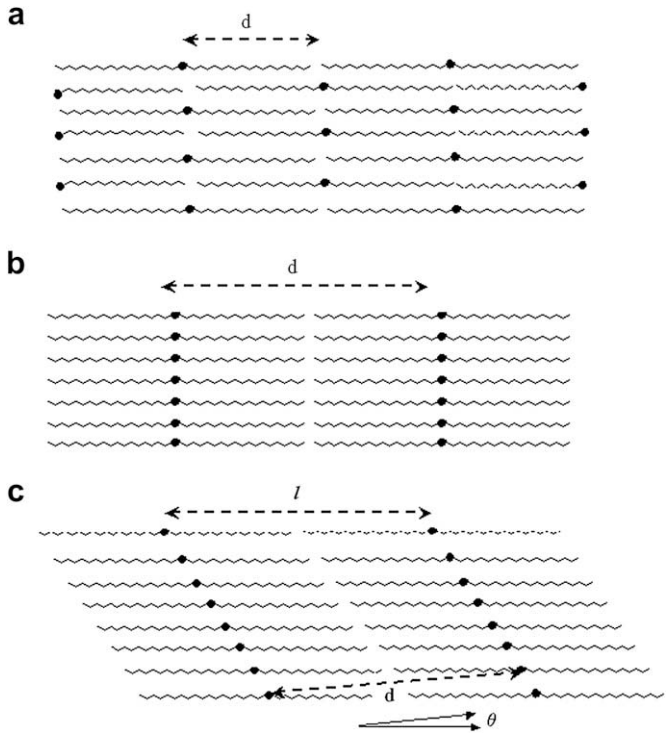

Fig. 9. Possible bilayer crystalline side-chain structures of ITA–SM copolymers. The polymer backbone is oriented normal to the plane of the page and represented by ●: (a) interdigitated; (b) non-interdigitated; (c) non-interdigitated with tilt (Parts (a) and (b) adapted from Ref. [18]).

[18]. For similar reason, the T_g was not resolved in the DSC curves of the ITA–SM copolymers with high SM concentration. The absence of a T_g in the DSC thermograms in this study is consistent with the work of Alig et al. [18] on the dynamics of side-chain crystalline comb-like polymers with a methacrylate polymer backbone and flexible side chains of stearyl methacrylate (SM) and perfluorododecyl methacrylate (PFM), both of which are crystallizable. The crystalline side chains form a bilayer structure with the polymer backbone sandwiched between crystalline layers of the side-chains, and although the backbone is flexible, its segmental mobility is suppressed until the side chain crystals melt (see X-ray discussion below). Thus, a T_g should only be detectable by DSC if it is above the melting point of the SM side chains. In fact, poorly resolved glass transitions were observed for copolymers with ITA concentration higher than 40 mol% (see the inset of Fig. 5 and Table 2), when $T_g > T_m$. The T_g values are compared with the prediction of the Fox-Flory equation for random copolymers [32] in Fig. 6. The T_g was composition dependent and approached that of PITA for high ITA concentrations. The T_g of PITA measured in this study was 120 °C, which is a lower than the value of 129 °C reported by Mormann and Feritz [33]. The Fox-Flory equation significantly underestimated the T_g of the copolymers, which is also a consequence of the stiffening of the backbone by the side-chain crystallinity.

The thermal stability of the PSM and PITA homopolymers and the ITA–SM copolymers is shown by the TGA data in Fig. 7. The PSM was thermally stable to ~270 °C, while the PITA began to degrade at about 170 °C. The PITA and the 70.1ITA–SM and 87.4ITA–SM copolymers exhibited a small mass loss prior to the primary degradation process, which is believed to be due to water evolution accompanying the anhydride ring reformation, i.e. the reverse reaction of the anhydride ring hydrolysis that may have occurred during handling of the polymer [12,33]. The PSM exhibited a two-step mass loss process (~270 and 315 °C), whereas the PITA showed three distinct degradation steps (~170, 265 and 370 °C). All of the copolymers showed three degradation steps, though the last step was closer to the 315 °C exhibited by PSM for copolymers with < 25 mol% ITA, but closer to ~340–350 °C for compositions with >25 mol% ITA.

Table 3
SAXS data for ITA–SM copolymers based on synchrotron X-ray measurement.

Copolymer	q_{max} (nm^{-1})	d (nm)
PSM	2.12	2.95
22.1ITA–SM	2.13	2.96
37.8ITA–SM	1.94	3.24
56.0ITA–SM	1.93	3.26
59.2ITA–SM	1.84	3.41
70.1ITA–SM	1.53	4.11
87.4ITA–SM	1.31	4.80

The PSM decomposed completely in nitrogen, but a significant amount, 19 wt%, of carbonaceous char residue remained at 900 °C for PITA. The amount of char remaining for the copolymers at 900 °C varied nonlinearly with the ITA concentration, see inset in Fig. 7 where a 3-parameter sigmoidal curve was used to fit the experimental data. The char is believed to be a condensed crosslinked structure formed by decarboxylation or decarbonylation of the anhydride ring, which needs oxygen to completely decompose [34]. High percentages of residue were also reported for the TGA of itaconic anhydride/methyl methacrylate copolymers [35], and Rice and Murphy [36] showed that ITA formed highly unsaturated isomers, propyne and allene, during pyrolysis, which could crosslink.

5. Structure of the SM side chains

WAXD data for PSM and the ITA–SM copolymers at temperatures below their respective melting points are shown in Fig. 8. The curve for PSM shows a relatively sharp diffraction peak at $q_{max} = 15.1\ nm^{-1}$ ($2\theta \sim 22^{\circ}$), which corresponds to an interchain spacing of $d = 0.416$ nm. A similar peak of lower intensity corresponding to $d = 0.414 - 0.416$ nm is seen for the copolymers. These data are consistent with the lattice spacing for hexagonally-packed paraffinic side chains, $d = 0.417$ nm [18,37], which confirms that the crystallinity of the ITA–SM copolymer originated from the SM side chains. The lower intensity and broadening of the peak as the ITA concentration increased is also consistent with the lower crystallinity in the copolymers, see the data in Table 2. The PITA sample was completely amorphous.

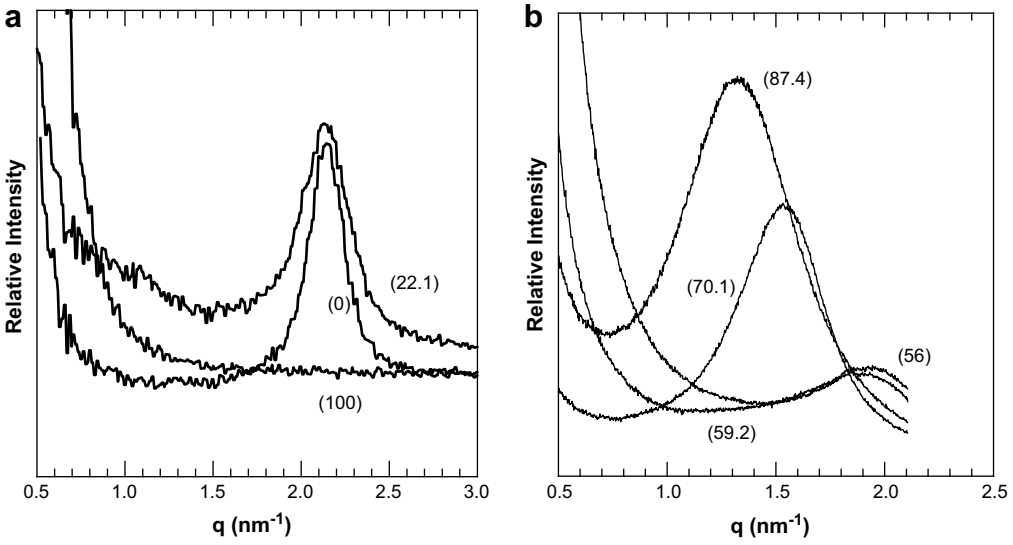

Fig. 10. SAXS curves for PSM, PITA and ITA–SM copolymers. The numbers in parentheses represent the mol% ITA in the polymer (zero corresponds to PSM, and 100 to PITA). (a), PSM, 22.1ITA–SM and PITA were measured at 23 °C using the Bruker, Anton-Paar SAXS instrument; (b) the rest of the copolymers were measured with synchrotron SAXS at −50 °C, to insure all were measured at semi-crystalline state.

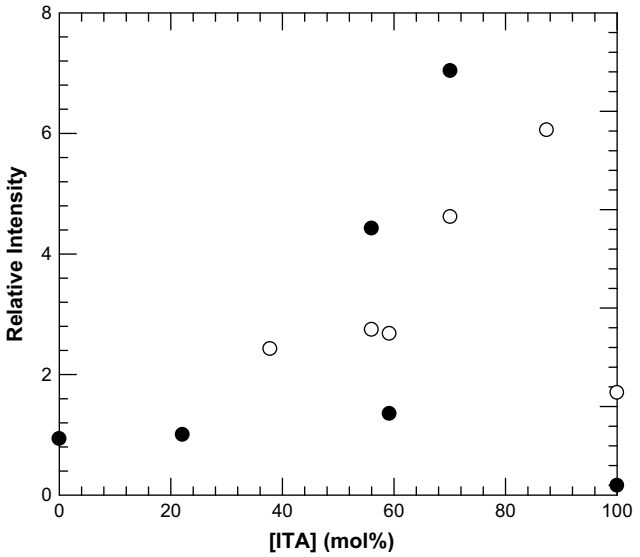

Fig. 11. SAXS intensity as a function of ITA concentration in the copolymers. (●) Bruker, Anton-Paar data; (○) BNL synchrotron data.

Polymers with comb-like paraffinic side chains are generally known to form layered structures [18,29,38–41], such as shown in Fig. 9. The side chains may be interdigitated (Fig. 9a) or non-interdigitated (Fig. 9b), and there may also be a tilt to the side chain packing as shown for the non-interdigitated case in Fig. 9c. In the latter case, the side chains pack at an angle to the main chain orientation, rather than normal as is shown in Fig. 9a and b. Although the schematics shown in Fig. 9 are drawn with the entire side chain in a *trans*-conformation (which is expected for the crystalline part of the chain), the entire alkyl chain does not participate in the crystal. The thermal analysis data in Table 2 that indicated less than 35% of the side-chain crystallized in the PSM and even less crystallized as the ITA concentration increased. That is expected because of the steric hindrance of the main chain, and as a result, the periodicity of the structure (denoted as *d* in Fig. 9, which measures the adjacent main chain to main chain distance) will generally be less than that calculated for an extended side chain (or twice the extended side chain for the non-intercalated or partially intercalated structures).

Prior studies of comb-like polymers with alkyl side chains tend to support the interdigitated side chain structure [18,37–40,42]. Plate [38] first proposed the interdigitated model based on the fact that the *d*-spacing followed a linear relation with the number of carbons (n) in the side chain,

$$d = d_o + kn \tag{3}$$

where d_o is the effective backbone diameter and the slope, k, represents the side-chain length increment per CH_2 group. More recent investigations [41,42] found that the side chains crystallized only when $n > 12$, but the average *d*-spacing increase per CH_2 group (k in equation (3)) was 0.13 nm, which coincides with the value for an extended alkyl chain (0.127 nm/CH_2). That result suggests an all *trans*-conformation of the alkyl side chain, even for the amorphous part. Shi and coworkers reached the same conclusion from FTIR studies [43].

The long-spacing, *d*, of the SM side-chains was measured by small-angle X-ray scattering (SAXS) on the polymers below T_m, see Fig. 10. The PSM homopolymer exhibited one broad peak at $q = 2.1\ nm^{-1}$, which corresponds to $d = 3.0$ nm. The position of the scattering maximum, q_{max}, decreased with increasing concentration of ITA, indicating a thicker SM phase. That may be a result of the increasing disorder due to the steric hindrance of the main chain when the SM units are spaced increasingly further apart in the copolymer. A fully extended stearate chain in an all-*trans* conformation has a $d \sim 2.5$ nm, which is less than the measured *d*-spacings listed in Table 3 for PSM and the ITA–SM copolymers. That eliminates the possibility of full interdigitation of the side chains, as shown in Fig. 9(a), but a 3–4 nm spacing can be achieved in a partially interdigitated model where only part of the chain crystallized. It is tempting to suggest a model for the microstructure wherein the interdigitated parts of the chain are crystalline and the region attached to the backbone is amorphous. Qualitatively, such a model is in agreement with the SAXS data that indicate the *d*-spacing of the side-chain phase increases with decreasing crystallinity – i.e., less interdigitation occurs with decreasing crystallinity.

The relative intensity of the SAXS peak for the copolymers, normalized by the intensity of the 22.1ITA–SM sample, is plotted in Fig. 11 for the data obtained from the two different SAXS instruments described in Experimental section. Although the crystallinity of the copolymers decreased with increasing ITA, the intensity of the SAXS peak increased, which is a consequence of

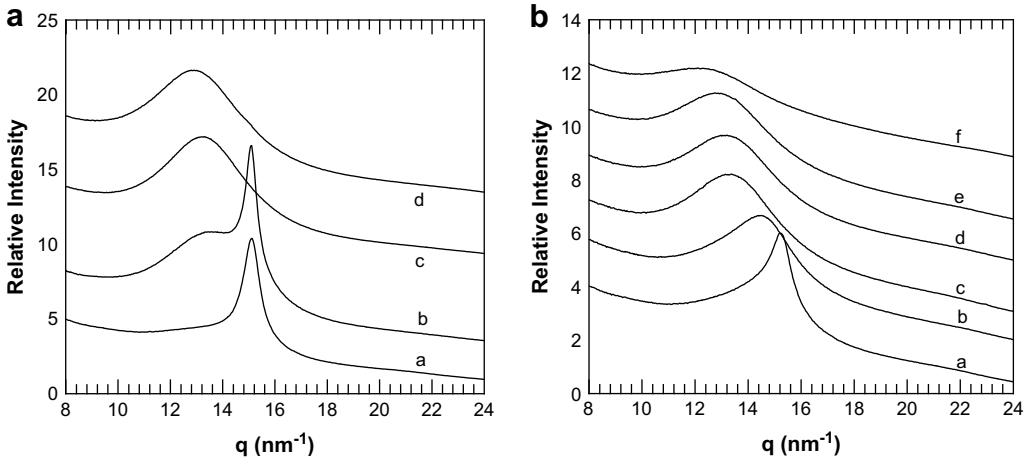

Fig. 12. WAXD (BNL synchrotron) curves for (a), PSM at $a = 20$ °C; $b = 30$ °C; $c = 40$ °C; $d = 100$ °C; and (b) ITA–SM59.2 at $a = -50$ °C; $b = 20$ °C; $c = 35$ °C; $d = 50$ °C; $e = 100$ °C; $f = 180$ °C. Data are displaced vertically for clarity.

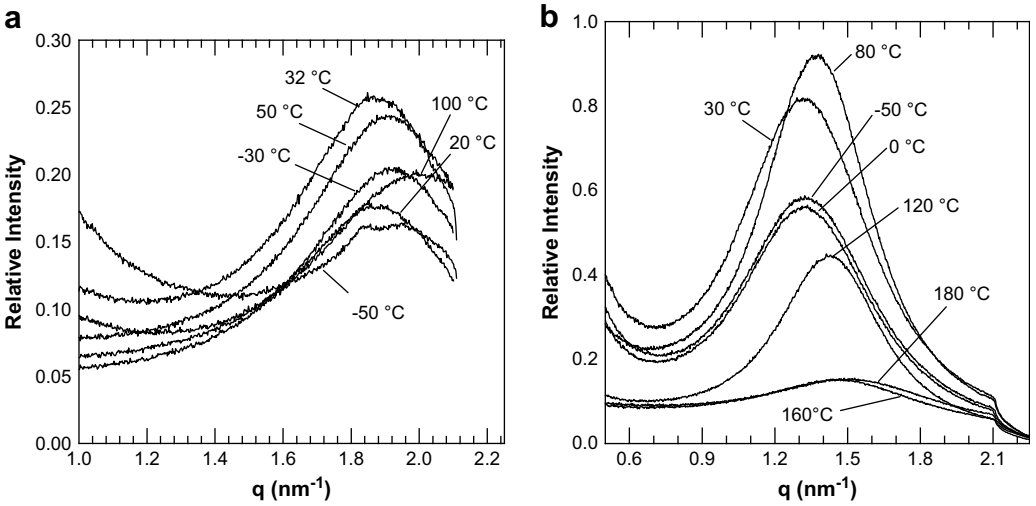

Fig. 13. SAXS for (a) ITA–SM37.8 ($T_m \sim 32\,^{\circ}C$, $T_g \sim 44\,^{\circ}C$) and (b) ITA–SM87.4 ($T_m \sim -22\,^{\circ}C$; $T_g \sim 110\,^{\circ}C$) as a function of temperature.

the higher electron density of ITA compared with SM. So, while the electron density of the SM phase decreased with decreasing crystallinity, the electron density contrast between the side-chain and matrix phases actually increased with increasing concentration of the more electron dense ITA. As a result, the SAXS intensity increased.

Temperature-resolved synchrotron WAXD and SAXS measurements were performed on the PSM and copolymers at the BNL synchrotron facility. Fig. 12 shows the WAXD data for PSM and 59.2ITA–SM at temperatures from below to above their melting points. The sharp crystalline PSM diffraction at $q_{max} = 15.1\ nm^{-1}$ ($d = 0.416$ nm) disappeared at the melting point ($\sim 30\,^{\circ}C$) and above 35 °C only an amorphous halo, centered at $q_{max} \sim 13.0\ nm^{-1}$ ($d = 0.488$ nm) was observed. For the 59.2ITA–SM sample, a sharp peak at $q_{max} = 15.1\ nm^{-1}$ reflects the crystallinity in the sample, but the amorphous halo is stronger in intensity, which is consistent with the lower crystallinity of the sample. In this case, the melting point was $\sim 6\,^{\circ}C$, see Table 2, and the crystalline peak disappeared between $-50\,^{\circ}C$ and room temperature (Unfortunately, the temperature intervals measured were too broad to resolve a precise melting point from the SAXS data).

For the temperature-resolved SAXS curves, however, the scattering peak did not disappear after melting of the side chains, see Fig. 13. Nanophase-separation of the amorphous side-chain persisted above T_m, which was probably due, in part, to the fact that $T_g > T_m$ for those copolymers and also, perhaps, due to immiscibility of the aliphatic side chain with the co-polyester. The characteristic size of the amorphous nanophase was essentially the same as for the semi-crystalline side-chain, as evidenced by the invariance of q_{max} in the SAXS curve below and above T_m. Similarly, the T_g appeared to have little or no effect on the size of the nanophase-separation of the amorphous side-chain. The intensity of the scattering, however, exhibited a complicated trend as temperature increased. The data in Fig. 13 indicate that the scattering intensity of the semi-crystalline copolymer increased as T_m was approached and continued to increase until the T_g of the copolymer. Above T_g, the intensity decreased, and the approach of the scattering intensity to zero as temperature further increased suggests an order–disorder transition in this system that would correspond to mixing of the side-chain and the backbone into a single phase. However, not enough temperatures were used to obtain data above T_g to allow calculation of an order–disorder transition temperature (T_{od}) in this study.

6. Thermomechanical behavior

TMA thermograms of the PSM, PITA and copolymers are shown in Fig. 14. With the exception of PITA, each sample exhibited one major softening transition and, in general, the transition temperature increased with increasing ITA content of the copolymers. The temperatures corresponding to 50% penetration, $T_{50\%,TMA}$, are listed in Table 2. The softening of the polymers reflects two different thermal transitions: 1) melting for PSM and copolymers with low ITA concentration (22.1ITA–SM and 37.8ITA–SM) and 2) a glass transition for copolymers with high ITA content and PITA. In general, the softening points, $T_{50\%,TMA}$, were $\sim 10\,^{\circ}C$ higher than the corresponding thermal transition measured by DSC, see Table 2. The low softening point of ITA–SM87.4 is believed to be a consequence of some thermal degradation that occurred while molding that sample at $\sim 160\,^{\circ}C$, which is close to its degradation temperature, see Fig. 7. The PITA sample used for Fig. 14 was solution-cast due to the degradation that occurred when molding the sample at elevated temperatures, as evidenced by discoloration of the sample. The TMA result for the PITA indicated a relatively high modulus at

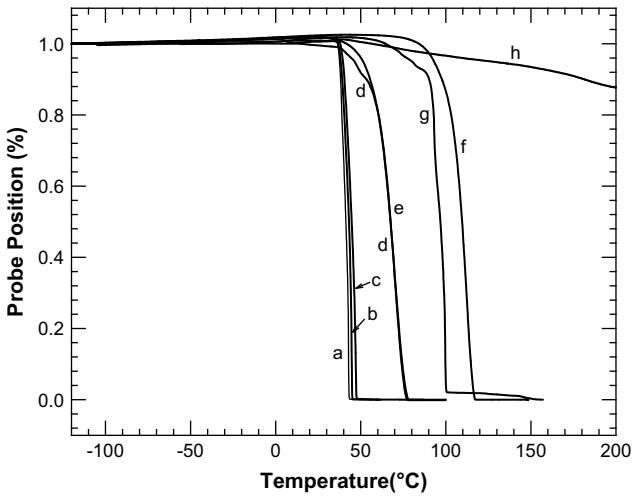

Fig. 14. TMA curves for PSM, PITA and ITA–SM copolymers. (a) PSM; (b) to (h) ITA–SM copolymers with ITA concentrations are 22.1, 37.8, 56, 59.2, 70.1, 87.4% respectively and PITA.

high temperatures, but no distinct T_g. The decrease in stiffness of PITA above 100 °C is due, in part, to its glass transition (~122 °C), but is also probably due to degradation of the sample.

7. Conclusions

Solution free-radical copolymerization of itaconic anhydride and stearyl methacrylate produces nearly random copolymers with a slight alternating tendency. These comb-like copolymers exhibit a nanophase-separated morphology, due to the incompatibility of the main chain and side-chains and by the crystallization of the side-chains. The alkyl side-chains crystallize into a hexagonal lattice, and the number of alkyl groups that participate in crystallization decreases with increasing separation of the side-chains. That is believed to be a consequence of the increasing difficulty in aligning the side-chains due to the steric hindrance from the backbone as the distance between side-chains increase and the requirement that the side chains must diffuse increasingly further to crystallize as their concentration decreases. The characteristic size of the nanodomains increases with increasing ITA concentration, which is probably due to the increasing frustration of packing the side-chains as the separation of the branches increases. The nanodomain morphology persists above the melting point of the side-chains.

The main chain mobility and side-chain crystallinity had competing effects on the thermal properties of the copolymers. Crystallization of the side-chains constrained the mobility of the main chain, which suppressed resolution of a T_g even though the backbone structure was relatively flexible. As the ITA concentration increased, the relatively stiff ITA component increased T_g, so that when $T_g > T_m$, a glass transition was observed. The incorporation of ITA increased the softening point of the copolymers, but it also decreased the thermal stability.

Acknowledgment

This work was funded by grants from the National Science Foundation and the U. S. Environmental Protection Agency, DMR-0328002-(TSE03-B), the New England Green Chemistry Consortium, which was supported by the U. S. Environmental Protection Agency and by the Green Chemistry Institute of the American Chemical Society, which is administered by the Petroleum Research Fund.

References

[1] Sinclair RG. Journal of Macromolecular Science, Pure and Applied Chemistry 1996;A33(5):585–97.
[2] Kulkarni RK, Pani KC, Neuman C, Leonard F. Polylactic acid for surgical implants. Archives of surgery (Chicago, Ill. 1960) 1966;vol. 93:839–43.
[3] Kinoshita K. Nippon Kagaku Kaishi (1921-47) 1929;50:583–93.
[4] Cayli G, Meier MAR. European Journal of Lipid Science and Technology 2008;110(9):853–9.
[5] Biermann U, Friedt W, Lang S, Luhs W, Machmuller G, Metzger JO, et al. Angewandte Chemie, International Edition 2000;39(13):2206–24.
[6] Meier MAR, Metzger JO, Schubert US. Chemical Society Reviews 2007;36(11):1788–802.
[7] Ishida S, Saito S. Journal of Polymer Science, Part A-1: Polymer Chemistry 1967;5(4):689–705.
[8] Papanu VD. Amide-imide derivatives of homopolymers of itaconic anhydride having antitumor activity. Application: EP. USA: Monsanto Co.; 1983. pp. 18.
[9] Yang JZ, Nakatsuka O, Otsu T. Chemistry Express 1990;5(10):805–8.
[10] Drougas J, Guile RL. Journal of Polymer Science 1961;55:297–302.
[11] Sharabash MM, Guile RL. Journal of Macromolecular Science, Chemistry 1976;A10(6):1033–48.
[12] Miles AF, Cowie JMG, Bennett RH, Brambley DR. Polymer 1991;32(3):484–8.
[13] Garrett ER, Guile RL. Journal of the American Chemical Society 1951;73:4533–5.
[14] Wallach JA. Biodegradable polymers derived from renewable resources: highly branched copolymers of itaconic anhydride. Polymer Science, vol. Ph.D. Storrs, CT: University of Connecticut, 2000.
[15] Wallach JA, Huang SJ. Biomacromolecules 2000;1(2):174–9.
[16] Kamagata K, Toyama M. Journal of Applied Polymer Science 1984;18:167–78.
[17] Ito K, Usami N. Macromolecules 1980;13:216–21.
[18] Alig I, Jarek M, Hellmann GP. Macromolecules 1998;31(7):2245–51.
[19] Mierzwa M, Floudas G, Stepanek P, Wegner G. Physical Review B Condensed Matter and Materials Physics 2000;62(21):14012–9.
[20] Milovanovic MB, Trifunovic SS, Katsikas L, Popovic IG. Journal of the Serbian Chemical Society 2007;72(12):1507–14.
[21] Tomic SL, Filipovic JM, Velickovic JS, Katsikas L, Popovic IG. Macromolecular Chemistry and Physics 1999;200(10):2421–7.
[22] Odian G. Principles of polymerization. 3rd ed. NY: Wiley Intersciences; 1991.
[23] Tate BE. Vinyl and diene monomers. NY: Wiley Interscience; 1970.
[24] Dinand E, Zloh M, Brocchini S. Australian Journal of Chemistry 2002;55(6 & 7):467–74.
[25] Flory PJ. Journal of Chemical Physics 1949;17:223–40.
[26] Flory PJ. Journal of Chemical Physics 1947;15(9):684.
[27] Iwahashi M, Takebayashi S, Taguchi M, Kasahara Y, Minami H, Matsuzawa H. Chemistry and physics of lipids 2005;133(2):113–24.
[28] Broadhurst MG. Journal of Research of the National Bureau of Standards, Section A Physics and Chemistry 1962;A66(No. 3):241–9.
[29] Hempel E, Huth H, Beiner M. Thermochimica Acta 2003;403(1):105–14.
[30] Leiva A, Gargallo L, Radic D. Journal of Macromolecular Science, Physics 1998;B37(1):45–57.
[31] Xu ZD, Song MS, Hadjichristidis N, Fetters LJ. Macromolecules 1981;14(5):1591–4.
[32] Fox Jr TG, Flory PJ, Marshall RE. Rubber Chemistry and Technology 1950;23:576–80.
[33] Mormann W, Ferbitz J. European Polymer Journal 2003;39(3):489–96.
[34] Velada J, Hernaez Z, Ceseros C, Karime I. Polymer Degradation and Stability 2004;52:273–82.
[35] Miles AF, Cowie JMG. European Polymer Journal 1991;27(2):165–70.
[36] Rice FO, Murphy MT. Journal of the American Chemical Society 1942;64:896–9.
[37] Floudas G, Stepanek P. Macromolecules 1998;31(20):6951–7.
[38] Plate NA, Shibaev VP. Journal of Polymer Science, Part D: Macromolecular Reviews 1974;8:117–253.
[39] Miller RL, Boyer RF, Heijboer J. Journal of Polymer Science, Polymer Physics Edition 1984;22(12):2021–41.
[40] Miller RL, Boyer RF. Journal of Polymer Science, Polymer Physics Edition 1984;22(12):2043–50.
[41] Hiller S, Pascui O, Budde H, Kabisch O, Reichert D, Beiner M. New Journal of Physics 2004;6:1–6.
[42] Hempel E, Budde H, Hoering S, Beiner M. Journal of Non-Crystalline Solids 2006;352(42–49):5013–20.
[43] Shi H, Zhao Y, Zhang X, Zhou Y, Xu Y, Zhou S, et al. Polymer 2004;45(18):6299–307.